chemosensors

Article

New Terbium Complex as a Luminescent Sensor for the Highly Selective Detection of Malathion in Water Samples

Moustafa A. Rizk [1,2,*], Mabkhoot A. Alsaiari [1], Raiedhah A. Alsaiari [1], Ibrahim A. Ibrahim [2], Abbas M. Abbas [2] and Gasser M. Khairy [2,*]

[1] Department of Chemistry, Faculty of Science and Arts at Sharurah, Najran University, Najran 68342, Saudi Arabia; mamalsaiari@nu.edu.sa (M.A.A.); raalsayari@nu.edu.sa (R.A.A.)
[2] Department of Chemistry, Faculty of Science, Suez Canal University, Ismailia 41522, Egypt; ibrahim_ali@science.suez.edu.eg (I.A.I.); abbasmamdoh@science.suez.edu.eg (A.M.A.)
* Correspondence: marizk@nu.edu.sa (M.A.R.); gasser_mostafa@science.suez.edu.eg (G.M.K.); Tel.: +966-560457015 (M.A.R.); +20-1022823954 (G.M.K.)

Abstract: A novel ligand, namely, (N′,N‴-((1E,2E)-1,2-diphenylethane-1,2-diylidene)bis(3-allyl-2-hydroxybenzohydrazide) (H2DBAZ), was designed and synthesized. This ligand demonstrated the ability to successfully interact with Tb(III) ions, resulting in the formation of a chemosensor that exhibited luminescent properties. The novel ligand was produced and subsequently subjected to characterization with several analytical techniques, including mass spectroscopy, elemental analysis, Fourier-transform infrared spectroscopy (FTIR), and proton nuclear magnetic resonance spectroscopy (^{1}H NMR). The postulated chemical structure of the Tb(III)–(DBAZ) complex was assessed utilizing a molar ratio approach. The chemosensor exhibited both selectivity and sensitivity towards malathion when compared to other nine organophosphorus pesticides that were investigated in methanol. The method was based on the phenomenon of luminescence static quenching shown by the complex subsequent to its interaction with the malathion pesticide. A linear Stern–Volmer plot was seen and, subsequently, utilized to generate the calibration curve. The observed linear range spanned from 0.39 to 60 μM, with a strong correlation coefficient of 0.999. Additionally, the limit of detection (LOD) was determined to be 0.118 μM. This methodology was successfully employed to measure the presence of malathion in various water samples. This particular complex exhibited promising potential for application in the development of a chemosensor utilizing the molecularly imprinted polymer approach.

Keywords: malathion; terbium; water samples; luminescence; organophosphorus pesticides

Citation: Rizk, M.A.; Alsaiari, M.A.; Alsaiari, R.A.; Ibrahim, I.A.; Abbas, A.M.; Khairy, G.M. New Terbium Complex as a Luminescent Sensor for the Highly Selective Detection of Malathion in Water Samples. *Chemosensors* **2023**, *11*, 570. https://doi.org/10.3390/chemosensors11120570

Academic Editor: Byoung Chan Kim

Received: 17 October 2023
Revised: 14 November 2023
Accepted: 23 November 2023
Published: 25 November 2023

1. Introduction

Pesticides are very important to the fast and efficient growth of agriculture because they protect crops as they grow and help store and move agricultural products [1]. Pesticides can be used to decrease the number of weeds and pests in order to enhance the agricultural product yield [2]. Moreover, even trace quantities of pesticide residues can dangerously pollute food, severely harm the natural environment, and endanger people's health [3–5]. The wide and excess use of pesticides has resulted in the presence of pesticide residues in drinking water and soil, which reaches the human body through the food chain. Therefore, pesticide contamination has become a major and important issue [6,7]. Malathion is an organophosphorus pesticide that has been extensively utilized in agriculture since 1950 [8]. The effectiveness of this compound in eliminating crop-damaging pests has led to their pervasive application in agricultural product enhancement [9,10]. However, the inaccurate use of malathion can result in a variety of environmental contaminations, including soil and water pollution, which further compromises the safety of food. From water bodies, it enters the food chain either through a direct or indirect way and, ultimately, causes damage to people and other aquatic beings.

In order to safeguard human wellness and the safety of industrial and agricultural employees, the Environmental Protection Agency (EPA) and the Food and Drug Administration (FDA) have regulated the utilization of malathion [11]. The EPA has determined that malathion is a class III (moderately hazardous) carcinogen. The FDA has established an 8 mg L^{-1} maximum residual limit (MRL) for malathion in food [12]. The World Health Organization (WHO) stated that more than a billion children suffer from diarrhea every year because they eat tainted food. This directly causes more than three million deaths from phosphate poisoning [13–15]. The toxic effects of pesticides are related to their efficiency in blocking acetylcholinesterase enzyme activity. This enzyme is crucial for the functioning of the nervous system, since it aids in the breakdown of acetylcholine, a neurotransmitter [16]. An excess of acetylcholine can lead to organ failure [17]. Within this context, the European Commission (EC) has set an overall MRL for pesticides in food at 0.01 mg/kg, while the FAO set an MRL of 1 mg/kg for malathion in fruit [18]. Hence, there is an immediate need for the precise detection and evaluation of organophosphorus pesticide residues in water to safeguard both food quality and human health [19].

The currently analytical methods for analyzing malathion and its derivatives depend heavily on chromatographic methods, such as GC [20], GC-MS [21–23], and HPLC [21,24]. Chromatographic analysis techniques offer a number of benefits, such as adequate sensitivity reaching parts per billion (ppb), high selectivity, and the ability to discriminate pesticides from complex samples; however, they also have drawbacks that are easily noticeable, including cumbersome sampling procedures and the expertise of trained technicians [25–27]. Therefore, there is an immediate need for quick, easy-to-use, and sensitive techniques for detecting pesticide residues in the real-world environment, such as chemosensors. The three main types of chemosensors based on the physical mechanism of sensing are thermal, electrical, and optical [28].

Optical chemical sensors provide many advantages over their electro-chemosensors, including greater selectivity, resistance to electromagnetic interference, and less risk of injury while handling potentially explosive compounds. Optrodes are similar to potentiometry, in that they can be used without a reference cell. They are also simple to miniaturize and can facilitate several investigations with a single set of control instruments [29]. Optical detection methods are fast, cheap, and easy to use. They are mostly used for detecting pesticides in a specific and sensitive way by monitoring changes in optical signals of different sources, like fluorescence, phosphorescence, SPR, SERS, and chemiluminescence [30]. The fluorescent technique is a more practical detection approach because of its high sensitivity, quick reaction speed, low detection limit, easy operation, and visible detection mode via eye vision [31,32]. Several research works highlight and describe recent developments in the field of luminescent-based optical sensors, and researchers are still working to create sensors with enhanced selectivity and sensitivity (lower LOD) for individual analytes, wider dynamic ranges, and the ability to monitor analyte concentrations in real time [33–36]. A variety of optical probes were devised to detect malathion using plasmonic nanoparticles, aptamers, enzymes, and other techniques [37–40]. However, certain approaches necessitate costly enzymes, intricate sample preparation procedures, and skilled operators to operate sophisticated instruments, thereby restricting their applicability. In addition to these efforts, the previous decade has also seen the development of luminescent lanthanide ions in optical chemosensors, specifically red- and green-emitting europium and terbium ions, respectively [41–44]. Chemosensors based on these ions have several benefits over conventional organic-based luminescent designs because of their unique photophysical features. The Tb(III) and Eu(III) complexes have some unique benefits, like being able to adjust the wavelength of excitation by choosing the ligand (chromophore) [45], good photochemical stability, a very narrow and strong emission band, and the capability to directly interact and coordinate with the analytes because of their large charge and size [46]. Further, their emission properties (lifetime, wavelength, and intensity) are more sensitive and affected by the compounds that bind to it [47]. These characteristics have led to great interest in optical sensor technologies that make use of lanthanides [48]. Adjusting the

selectivity capabilities of new Tb(III) or Eu(III) sensors is one of the most difficult parts of creating them. The most frequent methods for obtaining selectivity have included changing the structure and stoichiometry of the ligands bound to the lanthanide metal ions.

The luminescence of lanthanide ions is poor because of the Laporte forbidding character of the 4f transitions; as a result, their molar absorption coefficients are generally less than 3 M^{-1} cm^{-1} [49]. Sensitized emission, often known as the "antenna effect", is a method for indirectly exciting lanthanide ions [50]. This sensitization method allows for the characteristic emission of the lanthanide ion by transferring energy from an organic ligand (antenna (organic moiety)) to the lanthanide ion, thereby overcoming the restrictions that prevent the f–f transition of lanthanide ions. To achieve efficient sensitization, it is important to select an antenna whose triplet energy level is consistent with that of the lanthanide ion [51].

In the present work, a new ligand was synthesized, characterized, and used as an organic ligand (antenna) for Tb(III) to design a new luminescent lanthanide complex-based sensor. This innovative probe showed sensitive and selective detection of malathion pesticides. The determination was dependent on monitoring the luminescence quenching at 545 nm of the probe (characterized by Tb(III) ions) using an excitation wavelength of 360 nm in methanol. The probe showed selectivity and sensitivity towards malathion over other nine organophosphorus pesticides. Our probe showed the highest selectivity and sensitivity with a detection limit less than other previous probes and previous luminescent lanthanide probes [41–44]. The determination of malathion was based on static quenching. This approach was effectively used to quantify malathion in different water samples. This study is a continuation of our efforts to design molecularly imprinted polymer sensors containing luminescent Tb(III) or Eu(III) complexes that can be polymerizable, to show selectivity profiles for organophosphate pesticide analytes, and to find the optimal testing conditions for use as chemosensors in the identification of several classes of pesticides.

2. Materials and Methods

2.1. Materials

All chemicals and solvents were purchased from Sigma-Aldrich (St. Louis, MO, USA) (high-purity grade) and used without purification. The chemicals were as follows: terbium chloride hexahydrate ($TbCl_3.6H_2O$), 3-allyl-2-hydroxybenzohydrazide, and benzil. The heavy metal salts used were $Ni(NO_3)_2$, $Cd(NO_3)_2$, $Pb(NO_3)_2$, $CaCl_2$, NaCl, KCl, and NH_4Cl. Pesticides used included diazinon (A1), crotoxyphos (A2), chlorpyrifos (A3), chlorfenvinphos (A4), azinphos-ethyl (A5), phosdrin (A6), malathion (A7), heptachlor (A8), and endosulfan (A9) (Scheme S1). The solvents used were deionized water, methanol, ethanol, acetonitrile, and tetrahydrofuran (THF).

2.2. Instruments

The following instruments were used in this study: 1H NMR was performed on a Bruker Ascend 850 MHz (Bruker, Billerica, Massachusetts, USA). FTIR spectra was recorded in the 500–4000 cm^{-1} region through a Bruker FTIR Al-pha spectrometer (https://www.bruker.com, accessed on 2 August 2008). UV–VIS spectra were recorded using a Shimadzu UV-1800 spectrophotometer. (Shimadzu, Kyoto, Japan) (https://www.shimadzu.com, accessed on 5 May 2017). Emission spectra were obtained using a Jasco 6300 spectrofluorometer (Jasco, Tokyo, Japan) (https://jascoinc.com, accessed on 8 September 2010). The elemental analysis (CHN) was performed using an Elementar Varian EL instrument (Elementar, Langenselbold, Hesse, Germany). Mass spectra were obtained on a LTQ XL linear ion trap mass spectrometer (Thermo Scientific™, Waltham, MA, USA).

2.3. Ligand Preparation (H2DBAZ)

In total, (0.40 g, 2 mmol) of benzil in ethanol (25 mL) was gradually added to (0.80 g, 4 mmol) of 3-allyl-2-hydroxybenzohydrazide in ethanol (50 mL), which was synthesized according to Ibrahim et al. [40]. The reaction mixture was refluxed for 10 h. The precipitate

was collected, filtered, washed with ethanol, and then dried. Further purification was achieved through recrystallization from ethanol, resulting in a fine pale butter-yellow powder with a yield of 65%. It had a melting point of 180 °C (Scheme 1).

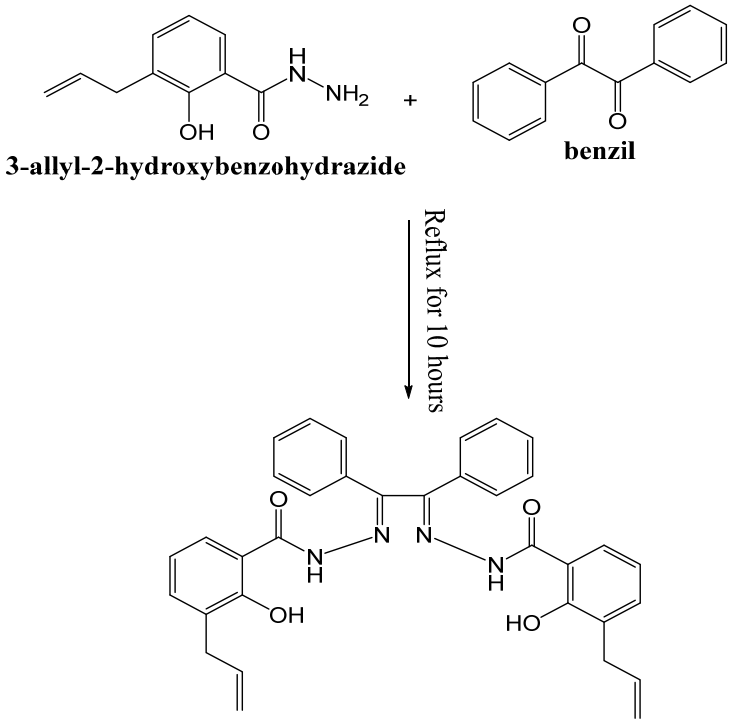

Scheme 1. Preparation of H2DBAZ.

Elemental analysis: calculated: (C, 73.10; H, 5.41; N, 10.03) found (C, 72.97; H, 5.63; N, 10.29). MS (ESI, positive mode): m/z = 558.64 [M]+, calculated mass for $C_{34}H_{30}N_4O_4$ 558.23 (Figure S1). ^{1}H NMR (DMSO, 400 MHz) δ ppm: 3.26–3.28 (m, 4 H, 2 CH_2), 4.95–5.04 (m, 4 H, 2 CH2), 5.96–6.06 (m, 2 H, 2 CH), 6.53–7.27 (m, 8 H, Ar-H), 7.42–7.76 (m, 8 H, Ar-H), 7.94 (bs, 2 H, 2 NH exchange with D_2O) (Figures S2 and S3). The IR bands were ν(O−H) phenolic 3397 cm^{-1}, ν(N−H) at 3255 cm^{-1}, ν(C=O) 1605 cm^{-1}, ν(C=N) 1575 cm^{-1}, δ(N−H) amide I band at 1393 cm^{-1} and δ(N−H) amide II band at 1338 cm^{-1} (Figure S4).

2.4. Solution Preparation

A total of 10^{-3} M stock solutions of Tb(III) ions, H_2DBAZ, and pesticides were prepared by dissolving a calculated amount of each in methanol. Working solutions were prepared by appropriately diluting stock solutions. Working solutions were freshly prepared daily. The complex was freshly prepared through mixing appropriate amounts of ligand and Tb(III) stock solutions and completing the working solution with methanol. The fluorescence intensity of the complex was tested throughout one hour (every 5 min). The complex showed good stability where the fluorescence intensity of the working solution was still constant within one hour. All of the solutions were kept in 4 °C and kept in the dark with the use of aluminum foil.

2.5. The Experimental Procedure

The emission spectra and luminescence intensities were recorded at an emission wavelength of 545 nm using an excitation wavelength of 360 nm. The effects of adding pesticides (0, 0.5, 1, 5, 10, 20, 40, and 60 μM) to the complex were studied in a 1 cm quartz cuvette. The molar ratio 1:1 of Tb(III)/H_2DBAZ was used for all the experiments. The

data obtained were analyzed using the Stern–Volmer equation, owing to the quenching effect. The type of luminescence quenching was investigated by plotting the titration data using the Stern–Volmer equation at various temperatures. Each measurement was repeated thrice, and the average value was calculated and recorded.

2.6. Sample Preparation

The water samples were collected from different regions in Ismailia city, Egypt. The samples were collected in 1 L glass containers. The samples were filtrated through a Whatman filter paper grade 1 circle (125 mm diam., thickness 180 µm, and 0.45 µM pore size) to remove the suspended wastes and solids. The pHs of the samples were adjusted in the range from 6.0 to 8.0 with 0.1 M sulfuric acid or sodium hydroxide. The samples were refrigerated at 4 °C until they were utilized. Due to the low levels of malathion in the water used in this investigation, a recovery study was conducted following the addition of the necessary amounts of malathion to real water samples. The extraction and analyses were conducted 24 h after malathion was added to the water from various sources.

The extraction of malathion from water samples was performed as follows: A sample of 100 mL of water was put into a 250 mL separatory funnel. The separatory funnel was shut after adding 20 mL of methylene chloride, then agitated for 1–2 min with occasional venting to release the pressure. The organic layer extract was obtained after the funnel had been left to sit for 10 min. Two further extractions were performed using new portions of methylene chloride. The extracts were dried with anhydrous sodium sulfate and heated until they were almost dry. The residue was dissolved with 1 mL of methanol and used for a spectrofluorimetric analysis.

3. Results and Discussion

3.1. Spectral Properties of the Chemosensor and Its Interaction with Malathion

3.1.1. UV–Vis Absorption Spectroscopy

The spectral properties of the ligand (H_2DBAZ) and its complex with the Tb(III) ions were studied using luminescence and UV–Vis absorption spectroscopy in methanol. H_2DBAZ showed two absorption bands at 249 and 298 nm due to the $\pi \rightarrow \pi^*$ ($\varepsilon_{249\,nm}$ = 10,520 ± 120 M^{-1} cm^{-1}) and $n \rightarrow \pi^*$ ($\varepsilon_{298\,nm}$ = 10,520 ± 120 M^{-1} cm^{-1}) transitions, respectively. The $n \rightarrow \pi^*$ band was attributed to the –OH, NH, C=O, and C=N groups. When treated with Tb(III), a blue and hypochromic shift of the bands was observed at 245 and 294 nm, respectively, proving the coordination between the H_2DBAZ and Tb(III) ions (Figure 1). Additionally, upon the addition of malathion (A7) to the Tb(III) complex, the band at 245 nm unchanged, while a blue shift on the absorption band of the complex at 294 to 288 nm with a slightly increased absorbance revealed the binding between the complex and the pesticide.

The effect of the solvents on the absorption of the ligand (H_2DBAZ) and its complex with the Tb(III) ions was tested, as shown in Figures S5 and S6. As the polarity of the solvents increased, there was a slight decrease in the wavelength (bathochromic shift). The presence and strength of the hydrogen bonds between the solvent molecules and spectrally active molecules affected the degree of spectral shift for these molecules. Hydrogen bonds usually present between the substituent groups of the spectrally active molecule and the –NH or –OH groups of solvent molecules [52]. Changes in the spectra are solvent-polarity-sensitive to molecules that lack intramolecular hydrogen bonds. Consequently, as the polarity of the solvent increases, the bands (π–π^*) of many molecules undergo a bathochromic shift. Hydrogen bonding between solute and solvent molecules is thought to be the cause of these shifts [53].

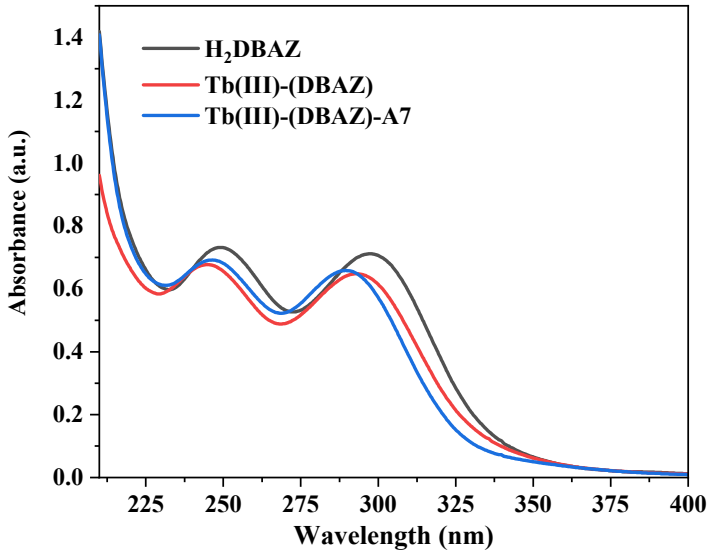

Figure 1. UV-vis spectra of 5×10^{-5} M H_2DBAZ (black line), 5×10^{-5} M Tb(III) + 5×10^{-5} M DBAZ (red line) and 5×10^{-5} M Tb(III) + 5×10^{-5} M DBAZ + 5×10^{-5} M A7 (blue line) in methanol at room temperature.

3.1.2. Luminescence Emission Spectroscopy

Figure 2a shows the fluorescence spectrum of H_2DBAZ in methanol at an excitation wavelength of 360 nm. H_2DBAZ exhibited an emission band at 437 nm in methanol. When the photochemically active group-containing molecule in methanol was excited at 300 nm, the nonbonding electrons were promoted to the π* orbital (n→π*) and then deactivated, resulting in an emission at 437 nm [54]. The luminescence excitation and emission spectra of Tb(III)–DBAZ in methanol are shown in Figure 2b. The excitation spectra of the Tb(III) complex were measured using the emission wavelength (λ_{em} = 545 nm) within the scanning range of 200–400 nm.

Additionally, the emission spectra of the probe were determined to be in the range of 400–750 nm at λ_{ex} = 360 nm. The characteristic luminescence peaks $^5D_4 \rightarrow {}^7F_6$ (490 nm), $^5D_4 \rightarrow {}^7F_5$ (545 nm), $^5D_4 \rightarrow {}^7F_4$ (587 nm) and $^5D_4 \rightarrow {}^7F_3$ (620 nm) transition of Tb(III) [55] were observed. The transition localized at 545 nm, which was the strongest, was hypersensitive and very sensitive to the coordinating environment. The probe was found to have a quantum yield (QY) of 0.61, which was calculated using the method as mentioned in reference [56].

The f–f absorption bands were extremely narrow due to the environment-related shielding of the 4f orbital by an outer shell of 5s and 5p orbits [57]. Tb(III) ions' excited states could be more densely populated by binding to organic ligands, which acted as a sensitizer. Lehn [58] used the term "antennas" to describe the ligands that exhibited this characteristic. These ligands in the lanthanide complex absorbed light and effectively transported it to the metal ion within the molecule, therefore, enhancing the luminescence of the complex. The energy transfer efficiency could be calculated from the change in the peak area for the emission spectra of the ligand before and after the complexation with the Tb(III) ion. The peak areas (A) of H_2DBAZ and the Tb(III)–DBAZ complex were 10,233 and 13, respectively, at λex = 360 nm in the range of 370–475 nm. The intramolecular energy transfer efficiency reached up to 99.87% ($1 - (A_{H2DBAZ}/A_{Tb(III)\text{-}DBAZ}) = 1 - (13/10{,}233 \times 100 = 99.87\%)$ [59]. It was proven that the ligand increased the luminescence intensity of the Tb(III) ion by transferring virtually all the absorbed energy to the Tb(III) ion.

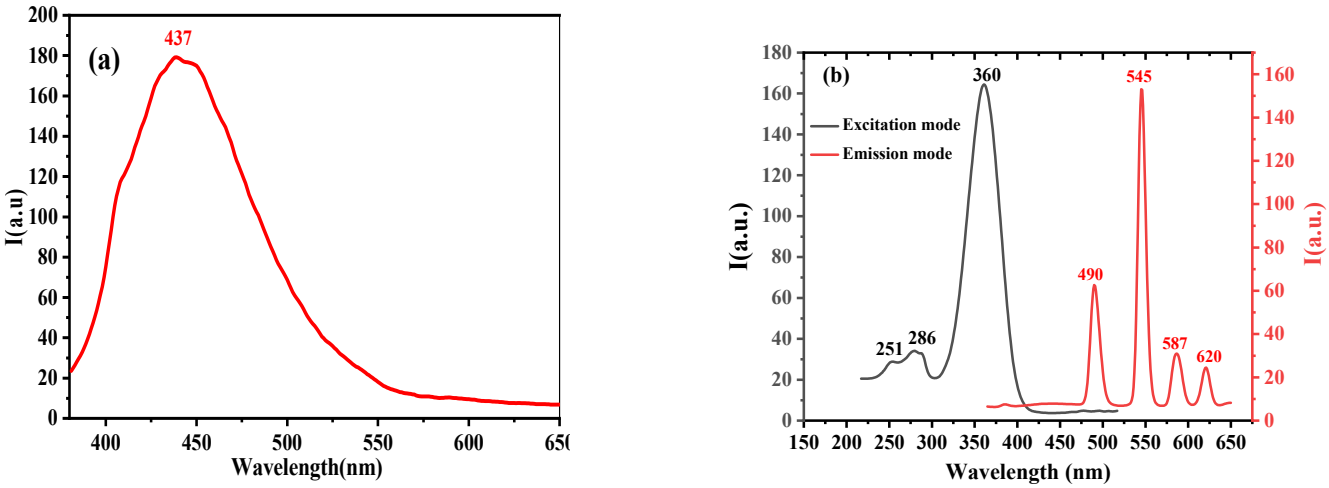

Figure 2. (**a**) Fluorescence spectra of 5×10^{-5} M H_2DBAZ in methanol at λ_{ex} = 360 nm. (**b**) The luminescence excitation and emission spectra of 5×10^{-5} M Tb(III)-DBAZ in methanol, sensitivity medium, and at room temperature using $\lambda_{ex/em}$ = 360/545 nm.

3.2. Solvent Effect

The influence of solvents on the luminescence intensities of the Tb(III) complex was investigated, and the result is given in Figure 3. Water quenched the emission of the Tb(III)–DBAZ complex because it could absorb the electronic excitation energy of terbium ions through the high-frequency vibrational overtones of the O–H bond of water [60]. The luminescence intensities of the complex in water, acetonitrile, ethanol, and methanol at λ = 545 nm were 10, 185, 263, and 555, respectively. As mentioned, the luminescence intensity of the complex increased in the order methanol > ethanol > acetonitrile > water and was inversely proportional to the polarity index of the solvent (water = 10.2; acetonitrile = 5.8; ethanol = 5.2; and methanol = 5.1) [61]. The polarity index is defined as a measure of the degree of interaction between the solvent and the polar solute. Thus, the luminescence intensity of the complex decreased as the degree of the solvent interaction increased. Physical interactions between solvents and ligands vary in the quantity of energy absorbed, thereby modifying the luminescence intensity of the probe [62]. Thus, solvents affected the excited state of the ligand, altering the energy gap between the triplet state of the ligand and the emission level of terbium ions, which influenced the energy transfer efficiency. As a result, the emission at 437 nm (ligand) changed when various solvents were used.

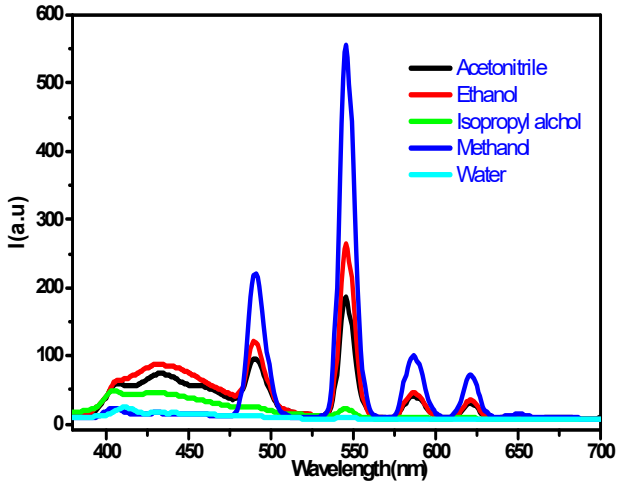

Figure 3. Luminescence spectra of 5×10^{-5} M Tb(III)–(DBAZ) complex in different solvents, λ_{ex} = 360 nm, sensitivity high, and at room temperature.

3.3. Complex Stoichiometry

The stoichiometry of the Tb(III) probe was evaluated using a molar ratio method. Figure 4a shows the luminescence intensity (on *y*-axis) vs. molar ratio ([H_2DBAZ]/[Tb(III)]) (on *x*-axis), in methanol at the emission wavelength of 545 nm and using an excitation wavelength of 360 nm. The molar ratio 1:1 showed the best emission intensity. Under these conditions, the hypothesized chemical structure of the Tb(III)–(DBAZ) complex is displayed in Figure 4b, where the ligand acted as a hexadentate ligand through four oxygen atoms and two nitrogen atoms and the coordination sphere was completed with two molecules of methanol. One chloride atom was present at the outer sphere of the complex.

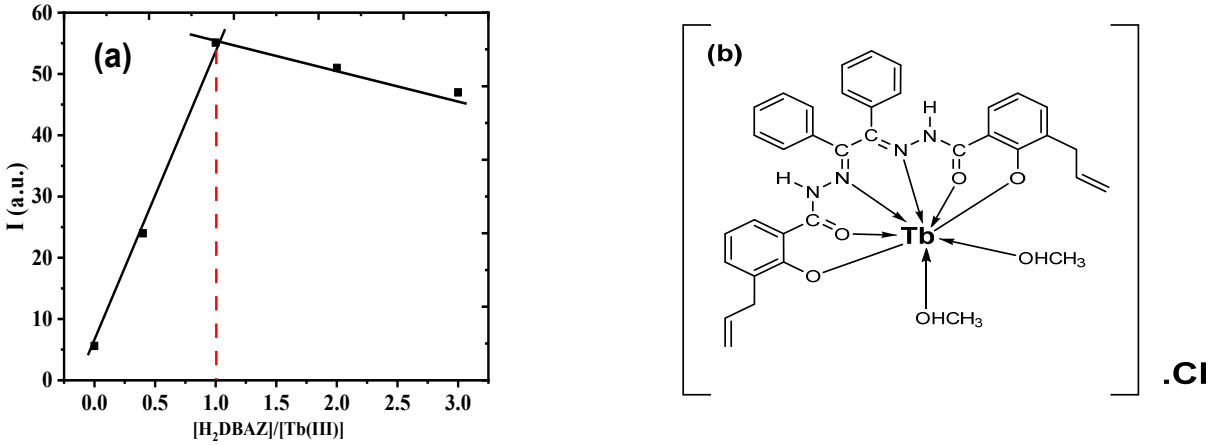

Figure 4. (**a**) Luminescence intensity of ligand/Tb(III) molar ratio at $\lambda_{ex/em}$ = 360/545 nm in methanol at room temperature ([Tb(III)] = 5 × 10^{-5} M; [H_2DBAZ] = 0, 2.5 × 10^{-5}, 5 × 10^{-5}, 1 × 10^{-4}, 1.5 × 10^{-4}); (**b**) the hypothesized structure of the Tb(III) complex.

3.4. Response Time

In order to determine the best time of measuring the luminescence intensity of the probe, the luminescence signal of the probe at 545 nm was monitored with time (Figure S7). It was observed that the signal increased with time to approximately 25 min of the start point, then stabilized. Based on this point, we performed all studies after mixing the Tb(III) ions and ligands for 30 min, at which point the luminescence reached its maximum value and became constant. This may be attributed to the complete binding between the Tb(III) ion and ligand, which permitted the effective transport of the absorbing light by the ligand to the metal ion within the molecule to be maximum.

3.5. Selectivity

The luminescence response of the 5 × 10^{-5} M of Tb(III) complex towards 5 × 10^{-5} M of pesticides (chlorfenvinphos, chlorpyrifos, phosdrin, azinphos-ethyl, dichlorvos, crotoxyphos, diazinon, isofenphos, malathion, paraoxon-ethyl, endosulfan, and heptachlor) in methanol is shown in Figure 5. The signal of the probe was quenched with malathion when compared with other pesticides at 545 nm. These results indicated that the probe detected malathion in methanol with greater sensitivity and selectivity. This may have been attributed to the selective complex formation between the probe and malathion. The binding was monitored via the alteration in the emission bands of the Tb(III) complex (especially 545 nm). It was also observed that the band at 470 nm due to the ligand (H_2DBAZ) was affected with different pesticides, which suggested that the ligand could be used as a chemosensor for organophosphorus pesticides under our investigation. The use of the luminescent lanthanide complex here as a probe had a higher advantage than the organic ligand, where the complex showed a characteristic spectra when compared to organic ligands, such as millisecond lifetimes, sharp emission spectra, and a higher quantum yield. Hence, the utilization of lanthanide-complex-based chemosensors presented a more advantageous

alternative compared to organic fluorophores, particularly in addressing challenges related to background autofluorescence [43].

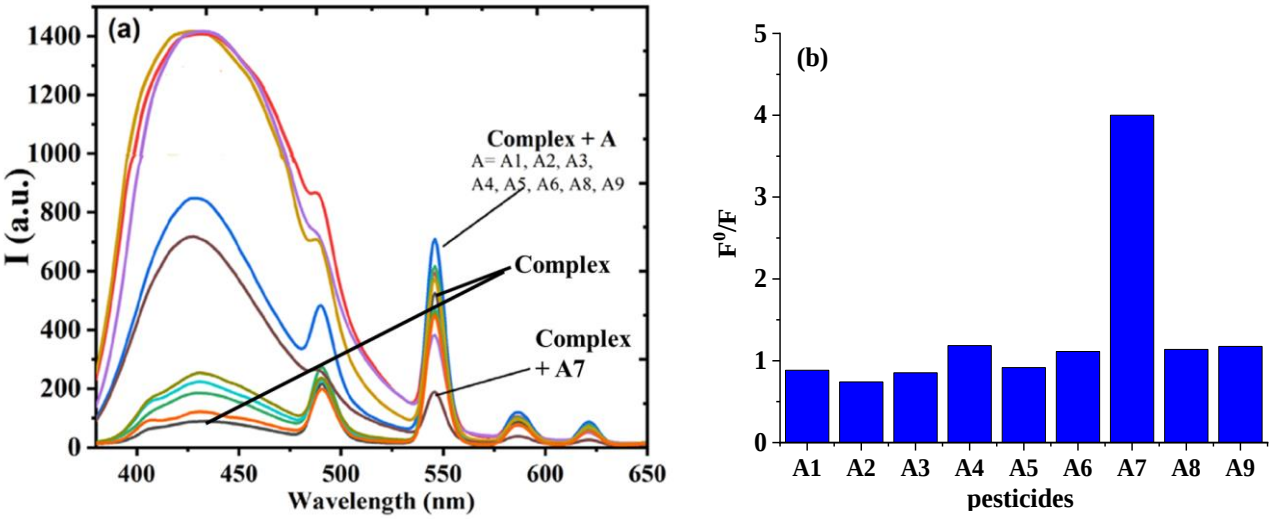

Figure 5. (**a**) Luminescence spectra of the interaction between 5×10^{-5} M of Tb(III)–(DBAZ) complex and 5×10^{-5} M of different pesticides in methanol, $\lambda_{ex/em}$ = 360/545 nm, high sensitivity at room temperature. (**b**) Histogram of F^0/F values versus organophosphorus pesticides under study, where F^0 and F are the luminescence intensity of the complex in the absence and present of the pesticides in methanol, respectively, $\lambda_{ex/em}$ = 360/545 nm, high sensitivity at room temperature. Diazinon (A1), crotoxyphos (A2), chlorpyrifos (A3), chlorfenvinphos (A4), azinphos-ethyl (A5), phosdrin (A6), malathion (A7), heptachlor (A8), and endosulfan (A9).

3.6. Calibration Curve

The emission spectra and calibration curve of 5×10^{-5} M of the Tb(III)–(DBAZ) complex with various concentrations of malathion (0, 0.5, 1, 5, 10, 20, 40, and 60 µM) in methanol, λ_{ex} = 360 nm, are display in Figure 6. The emission intensity measurements of the complex with various concentrations of malathion displayed a quenching at the emission peak of the Tb(III) ion (λ_{em} = 545 nm). Plotting F^0/F against (A7) gave a straight line until a concentration of 60 µM with a regression equation $F^0/F = 1.003 + 0.042$ (A7) µM (Figure 6b). The linear range of the calibration curve was 0.39–60 µM with the correlation coefficient of R^2 = 0.999. The accuracy was 101.52% (n = 8). The limit of detection (LOD) and the limit of quantification (LOQ) were 0.118 and 0.39 µM, respectively. The LOD and LOQ were obtained using the following equations:

$$LOD = 3\delta/slope \quad (1)$$

$$LOQ = 10\delta/slope \quad (2)$$

in which δ is the standard deviation of the blank containing 5.00×10^{-5} M of the Tb(III)–(DBAZ) complex in methanol. Table 1 includes a simple comparison between our probe and some other lanthanide-based probes, all used in detecting malathion. Our probe showed a lower detection limit than other probes [41–44].

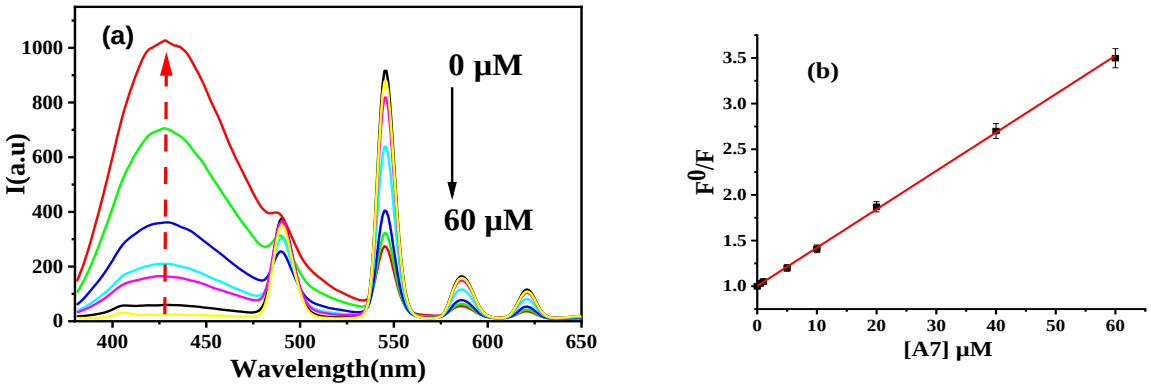

Figure 6. (**a**) Emission spectra of 5×10^{-5} M of Tb(III)–(DBAZ) complex with various concentrations of malathion (p6) in methanol, sensitivity high, λ_{ex} = 360 nm, λ_{em} = 545 nm, and at room temperature. (**b**) Calibration plot for malathion (A7) after its interaction with 5×10^{-5} M of Tb(III)–(DBAZ) complex in methanol medium, $\lambda_{ex/em}$ = 360/545 nm, and at 25 °C.

Table 1. An evaluation of Tb(III)–(DBAZ) probe compared with some chemosensors for malathion detection.

Probe	Limit of Detection	Interferent Pesticides	Medium of Detection	Reference
Tb(III)- N′,N‴-((1E,2E)-1,2-diphenylethane-1,2-diylidene)bis(3-allyl-2-hydroxybenzohydrazide	0.118 µM	-------	Methanol	This work
Tb(III)-ethyl-4-hydroxy-1-(4-methoxyphenyl)-2-oxo-1,2-dihydroquinoline-3-carboxylate	0.94 µM in ethanol 2.68 µM in water	Crotoxyphos	Ethanol or water	[41]
Tb(III)-N(acetoacetyl)-3-allyl-2-hydroxy benzaldehyde hydrazone	9.59 µM	Chlorfenvinphos	Ethanol	[42]
Eu(III)–1,10 phenanthroline-4,4,4-trifluoro-1-(2-naphthyl)-1,3-butanedione	0.64 µM	Chlorpyrifos endosulfan, heptachlor	HEPS buffer (pH = 7.5)	[43]
Eu(III)–2,6-pyridinedicarboxylic acid	2.50 µM	Azinphos chlorfenvinphos	HEPS buffer (pH = 7.5)	[44]

3.7. Mechanism of Quenching

The emission intensity of the Tb(III) complex exhibited a consistent reduction as the concentration of malathion steadily increased. This observation suggested a potential interaction among the complex and malathion. The major reason for the observed quenching of the probe could be attributed to the formation of an adduct between the ground state Tb(III) complex and malathion, or, alternatively, to collisional quenching. The linear relationship between the ratio of F^0/F and malathion concentration, as seen in Figure 6a, exhibited a positive correlation. This correlation may be accurately described by a linear regression equation that adhered to the Stern–Volmer equation.

$$F^0/F = 1 + Ksv\,[Q] = 1 + Ka\,[Q] \quad (3)$$

Ksv is the Stern–Volmer constant. Under specific conditions [63] for static quenching, the Stern–Volmer constant can be replaced with the thermodynamic association constant Ka.

The plot generated using the Stern–Volmer equation did not exhibit any departure towards the y-axis throughout the experimental concentration range under investigation. This observation suggested that either static or dynamic quenching was the main mechanism.

The distinction between static and dynamic quenching may be discerned based on their respective dependencies on temperature and excited-state lifetime. The phenomenon of dynamic quenching can be classified as being diffusion-controlled due to the requirement for the quencher to undergo a diffusion towards the fluorophore during the lifetime of the excited state's existence. The diffusion coefficient was anticipated to rise at elevated temperatures, leading to a corresponding increase in the bimolecular quenching constants. If the value of K dropped as the temperature increased, it could be inferred that the quenching process was characterized by a static nature rather than a dynamic one. Static quenching is characterized by the presence of an effective quenching sphere or the formation of a nonluminescent complex in the ground state. On the other hand, collisional or dynamic quenching occurs when an excited-state fluorophore and a ground-state quencher collide, leading to the formation of a transient complex. The complex in the excited state undergoes dissociation through both radiative and nonradiative deactivation processes.

The mechanism was confirmed by studying the effect of temperature on the interaction between the malathion and the probe (Tb(III)–(DBAZ)) by monitoring its luminescence intensity and plotting the Stern–Volmer equation at various temperatures (Figure S8). Table 2 shows that the Stern–Volmer binding constant (K_{sv}) was inversely proportional to the temperature. This could be considered evidence for the probable quenching of malathion–Tb(III)–(DBAZ) luminescence through a binding reaction, which was initiated through ground-state compound formation rather than dynamic collision. The quenching plots illustrated that the quenching of the emission of the Tb(III) complex was in good agreement with the linear Stern–Volmer equation. Increasing the temperature usually causes the dissociation of weakly bound compounds. Therefore, chelation-enhanced luminescence quenching (CHEQ) may give us a simple explanation for the luminescence quenching of the complex [64,65]. Therefore, the malathion was coordinated to the probe through the functional thiophosphoryl group (P=S) or carbonyl group (C=O); this chelation formed a nonluminescent complex, causing a quenched luminescence signal.

Table 2. Stern–Volmer constants of the interaction between Tb(III) complex and malathion pesticide.

Temp. (K)	Correlation Coefficient (r)	Ksv (Slope) (M^{-1})
298	0.999	4.20×10^4
303	0.998	4.04×10^4
308	0.995	3.72×10^4
313	0.988	3.09×10^4
318	0.948	2.54×10^4

3.8. Thermodynamic Parameters

At various temperatures (303, 308, 313, and 318 K), the Lineweaver–Burk plot was utilized to compute the binding constants (K) [66]; the data are collected in Table 3. The thermodynamic parameters ΔH^o and ΔS^o were evaluated for the additional characterization of the contact between the Tb(III)–(DBAZ) probe and malathion using the Van 't Hoff equation [67]:

$$Ln\ K = -\frac{\Delta H}{RT} + \frac{\Delta S}{R} \quad (4)$$

The value and sign of (ΔH^o) and (ΔS^o) were significant evidence for confirming the binding modes. A positive ΔH^o and ΔS^o would indicate a hydrophobic interaction and a negative ΔH^o and ΔS^o would reflect the Van der Waals force or hydrogen bond. In contrast, negative ΔH^o and positive ΔS^o would suggest an electrostatic force [68].

The free energy (ΔG^{o}) was calculated using:

$$\Delta G^{0} = -RT\ lnK \quad (5)$$

The data are given in Table 3 and Figure 7 and Figure S9. The binding constant decreased as the temperature rose, suggesting that the interaction of malathion with the probe was exothermic. The negative value of ΔG^{o} and ΔH^{o} and the positive value of ΔS^{o} indicated that an electrostatic force played a significant role in the binding and the reaction was spontaneous [69].

Table 3. Thermodynamic parameter associated with the interaction of malathion (A7) with 5×10^{-5} mol/L of Tb(III)–(DBAZ) in methanol medium.

Temp. K	Binding Constant K (M^{-1})	R^2	ΔH^0 (KJ mol^{-1})	ΔS^0 (J mol^{-1}. K^{-1})	ΔG^0 (KJ mol^{-1})
303	4.80×10^4	0.979	−13.94	43.23	−26.03
308	4.20×10^4	0.981			−25.77
313	3.80×10^4	0.999			−24.04
318	3.40×10^4	0.998			−24.32

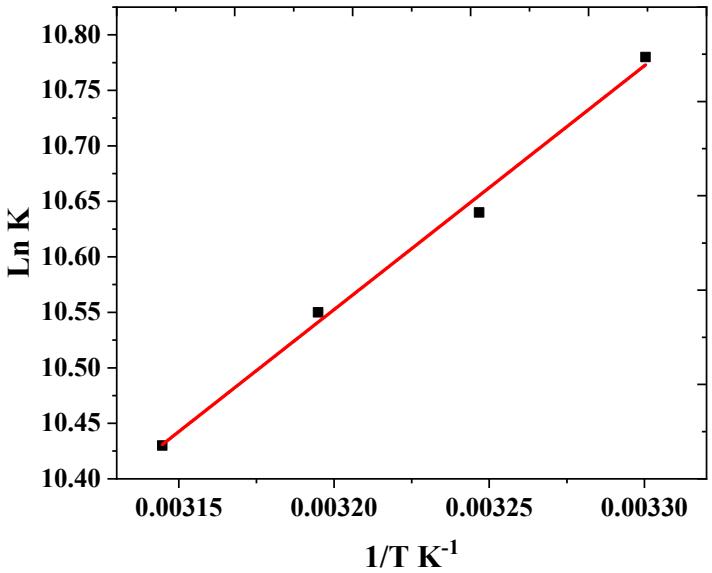

Figure 7. LnK against 1/T plot of the interaction of malathion (A7) with 5×10^{-5} mol/L of Tb(III)–(DBAZ) complex in methanol medium.

3.9. Interfering Species

Various interferents were used to investigate the interfering effect on the luminescence intensity of the probe in the presences of 20 μM of malathion pesticide. The effect of other frequently applied pesticides, e.g., heptachlor, chlorpyrifos, paraoxon-ethyl, and dichlorvos, on the malathion determination was also examined. The results are collected in Table 4. The tolerant concentration of the interferents was determined at a ±5% deviation from the mean luminescence intensity of the probe in the presence of a fixed concentration of malathion pesticide.

Table 4. The tolerant concentration of interference in the presence of 20 μM malathion in methanol.

Interferents	The Tolerant Concentration (μM)
Cu^{2+}	25 [Q]
Pb^{2+}	50 [Q]
Ni^{2+}	30 [Q]
Co^{2+}	80 [Q]
Cd^{2+}	40 [Q]
NO_3^-	50 [Q]
CO_3^{2-}	10 [Q]
PO_4^{3-}	10 [E]
Heptachlor	80 [Q]
Chlorpyrifos	100 [E]
Dichlorvos	100 [Q]
Paraoxon-ethyl	60 [Q]

Q: luminescence quenching effect. E: luminescence enhancement effect.

3.10. Application

Several types of water (river, tap, and waste) were tested for the insecticide malathion using the suggested approach in methanol. Mixed standard solutions of malathion were added to the water samples (the spiked concentrations were 10 and 20 μM) to investigate the spiked rates of the recovery of malathion pesticide. The results are presented in Table 5. Standardized addition statistics were used to evaluate the precision and reliability of the proposed approach [70]. Table 5 shows the recovery percentages, which were between 93.20% to 108.95%, with an average of 101.07% (based on three separate analyses), meeting the standards for a routine analysis detection. The RSD values were between 25.2% and 4.36%, which was in compliance with requirements of the stability.

Table 5. Recovery data of malathion in different water samples.

Water Sample	Added (μM)	Found (μM)	Recovery (%)	RDS (%)
Tap water	10.00	9.53	95.30%	2.52
	10.00	9.62	96.20%	
	10.00	9.55	95.50%	
	20.00	20.41	102.05%	
	20.00	20.70	103.50%	
	20.00	21.79	108.95%	
River water	10.00	9.85	98.50%	4.36
	10.00	9.70	97.00%	
	10.00	10.16	101.60%	
	20.00	19.59	97.95%	
	20.00	19.78	98.90%	
	20.00	21.77	108.85%	
Wastewater	10.00	10.30	103.00%	3.57
	10.00	9.80	98.00%	
	10.00	9.32	93.20%	
	20.00	21.20	106.00%	
	20.00	19.20	96.00%	
	20.00	19.19	95.95%	

4. Conclusions

A simple, luminescence-based chemosensor was developed for malathion determination using a Tb(III) complex. A new ligand was synthesized and characterized using FT-IR, ^{1}H NMR, and elemental analysis. Malathion was detected in methanol. The determination was dependent on monitoring the quenching of the luminescence intensity at 545 nm of the probe (characterized by Tb(III) ions). The quenching mechanism was static through

chelation-enhanced luminescence quenching (CHEQ) between malathion and the probe. The calibration curve was developed utilizing the Stern–Volmer equation. The linear range was between 0.39 and 60 μM, and the correlation coefficient was 0.999, while the LOD was 0.118 μM. The thermodynamic parameters were calculated and inferred that the binding was an electrostatic force of spontaneous origin and involved an exothermic process. The approach was effectively used to quantify malathion in different samples of water. More studies should be conducted to create molecularly imprinted polymer (MIP) fiberoptic sensors that can directly monitor samples of organophosphates pesticides.

Supplementary Materials: The following supporting information can be downloaded at: https://www.mdpi.com/article/10.3390/chemosensors11120570/s1, Figure S1: mass spectrum of the ligand; Figure S2: ^{1}HNMR of the ligand in DMSO-d6; Figure S3: ^{1}HNMR of the ligand in DMSO-d6 + D_2O; Figure S4: IR spectrum of the ligand; Figure S5: UV spectra of 5×10^{-5} M H_2DBAZ in different solvents at room temperature; Figure S6: UV spectra of 5×10^{-5} M Tb(III)-DBAZ complex in different solvents at room temperature; Figure S7: effect of time on the luminescence intensity of 5×10^{-5} M of Tb(III)–(DBAZ) complex in methanol medium, sensitivity high, λ_{ex} = 360 nm.; Figure S8: F^0/F against [A7] for malathion upon its interaction with 5×10^{-5} M of Tb(III)–(DBAZ) complex in methanol at different temperatures, λ_{ex} = 360 nm; Figure S9: $1/F_0$-F against 1/[pesticide] for malathion (A7) upon its interaction with 5×10^{-5} M of Tb(III)–(DBAZ) at different temperatures, (a) at 303 K, (b) at 308 K, (c) at 313 K, and (d) at 318 K.

Author Contributions: Conceptualization, G.M.K., M.A.R. and A.M.A.; methodology, G.M.K., I.A.I. and A.M.A.; validation, G.M.K. and A.M.A.; formal analysis, G.M.K. and A.M.A.; investigation, G.M.K., M.A.R., M.A.A., R.A.A., I.A.I. and A.M.A.; data curation, G.M.K., M.A.R. and A.M.A.; writing—original draft preparation, G.M.K., M.A.R., I.A.I. and A.M.A.; writing—review and editing, M.A.A. and R.A.A.; supervision, M.A.A. and R.A.A.; project administration and funding acquisition, M.A.R., M.A.A. and R.A.A. All authors have read and agreed to the published version of the manuscript.

Funding: This research was funded by the Deanship of Scientific Research at Najran University (grant number NU/DRP/SERC/12/1).

Institutional Review Board Statement: Not applicable.

Informed Consent Statement: Not applicable.

Data Availability Statement: All data generated or analyzed during this study are included in this published article (and its supplementary information files).

Acknowledgments: The authors are thankful to the Deanship of Scientific Research at Najran University for funding this work under the General Research Funding program.

Conflicts of Interest: The authors declare no conflict of interest.

References

1. Chen, Y.; Liu, H.; Tian, Y.; Du, Y.; Ma, Y.; Zeng, S.; Gu, C.; Jiang, T.; Zhou, J. In Situ Recyclable Surface-Enhanced Raman Scattering-Based Detection of Multicomponent Pesticide Residues on Fruits and Vegetables by the Flower-like MoS_2@Ag Hybrid Substrate. *ACS Appl. Mater. Interfaces* **2020**, *12*, 14386–14399. [CrossRef]
2. Wang, J.; Zhang, J.; Wang, J.; Fang, G.; Liu, J.; Wang, S. Fluorescent Peptide Probes for Organophosphorus Pesticides Detection. *J. Hazard. Mater.* **2020**, *389*, 122074. [CrossRef]
3. Carvalho, F.P. Pesticides, Environment, and Food Safety. *Food Energy Secur.* **2017**, *6*, 48–60. [CrossRef]
4. Singh, R.; Kumar, N.; Mehra, R.; Kumar, H.; Singh, V.P. Progress and Challenges in the Detection of Residual Pesticides Using Nanotechnology Based Colorimetric Techniques. *Trends Environ. Anal. Chem.* **2020**, *26*, e00086. [CrossRef]
5. Lu, Y.; Wei, M.; Wang, C.; Wei, W.; Liu, Y. Enhancing Hydrogel-Based Long-Lasting Chemiluminescence by a Platinum-Metal Organic Framework and Its Application in Array Detection of Pesticides and d-Amino Acids. *Nanoscale* **2020**, *12*, 4959–4967. [CrossRef]
6. Tang, F.H.M.; Lenzen, M.; McBratney, A.; Maggi, F. Risk of Pesticide Pollution at the Global Scale. *Nat. Geosci.* **2021**, *14*, 206–210. [CrossRef]
7. Zhou, B.; Li, X. The Monitoring of Chemical Pesticides Pollution on Ecological Environment by GIS. *Environ. Technol. Innov.* **2021**, *23*, 101506. [CrossRef]

8. Irfan Azizan, M.A.; Taufik, S.; Norizan, M.N.; Abdul Rashid, J.I. A Review on Surface Modification in the Development of Electrochemical Biosensor for Malathion. *Biosens. Bioelectron. X* **2023**, *13*, 100291. [CrossRef]
9. Lai, X.; Zhang, S.; Du, G.; Wang, Y.; Han, Y.; Ye, N.; Xiang, Y. Ultrasensitive Determination of Malathion in Apples by Aptamer-Based Resonance Scattering. *Anal. Lett.* **2021**, *54*, 1639–1653. [CrossRef]
10. Aghoutane, Y.; Diouf, A.; Österlund, L.; Bouchikhi, B.; El Bari, N. Development of a Molecularly Imprinted Polymer Electrochemical Sensor and Its Application for Sensitive Detection and Determination of Malathion in Olive Fruits and Oils. *Bioelectrochemistry* **2020**, *132*, 107404. [CrossRef] [PubMed]
11. *Toxicological Profile for Malathion*; Agency for Toxic Substances and Disease Registry (ATSDR): Atlanta, GA, USA; United State Department of Health & Human Services: Atlanta, GA, USA; Public Health Services: Atlanta, GA, USA, 2003.
12. Chen, Q.; Sheng, R.; Wang, P.; Ouyang, Q.; Wang, A.; Ali, S.; Zareef, M.; Hassan, M.M. Ultra-Sensitive Detection of Malathion Residues Using FRET-Based Upconversion Fluorescence Sensor in Food. *Spectrochim. Acta A Mol. Biomol. Spectrosc.* **2020**, *241*, 118654. [CrossRef] [PubMed]
13. Phopin, K.; Tantimongcolwat, T. Pesticide Aptasensors—State of the Art and Perspectives. *Sensors* **2020**, *20*, 6809. [CrossRef] [PubMed]
14. Khatib, I.; Horyn, O.; Bodnar, O.; Lushchak, O.; Rychter, P.; Falfushynska, H. Molecular and Biochemical Evidence of the Toxic Effects of Terbuthylazine and Malathion in Zebrafish. *Animals* **2023**, *13*, 1029. [CrossRef] [PubMed]
15. Elmorsy, E.; Al-Ghafari, A.; Al Doghaither, H.; Salama, M.; Carter, W.G. An Investigation of the Neurotoxic Effects of Malathion, Chlorpyrifos, and Paraquat to Different Brain Regions. *Brain Sci.* **2022**, *12*, 975. [CrossRef]
16. Vasimalai, N.; Abraham John, S. Biopolymer Capped Silver Nanoparticles as Fluorophore for Ultrasensitive and Selective Determination of Malathion. *Talanta* **2013**, *115*, 24–31. [CrossRef] [PubMed]
17. Uygun, U.; Özkara, R.; Özbey, A.; Koksel, H. Residue Levels of Malathion and Fenitrothion and Their Metabolites in Postharvest Treated Barley during Storage and Malting. *Food Chem.* **2007**, *100*, 1165–1169. [CrossRef]
18. Vettorazzi, G. Pesticide Residues in Food in the Context of Present and Future International Pesticide Managerial Approaches. In *Pesticide Management and Insecticide Resistance*; Elsevier: Amsterdam, The Netherlands, 1977; pp. 97–128.
19. Liu, M.; Wei, J.; Wang, Y.; Ouyang, H.; Fu, Z. Dopamine-Functionalized Upconversion Nanoparticles as Fluorescent Sensors for Organophosphorus Pesticide Analysis. *Talanta* **2019**, *195*, 706–712. [CrossRef]
20. Tazarv, M.; Faraji, H.; Moghimi, A.; Azizinejad, F. Bursting-bubble Flow Microextraction Combined with Gas Chromatography to Analyze Organophosphorus Pesticides in Aqueous Samples. *J. Sep. Sci.* **2021**, *44*, 2965–2971. [CrossRef]
21. Harshit, D.; Charmy, K.; Nrupesh, P. Organophosphorus Pesticides Determination by Novel HPLC and Spectrophotometric Method. *Food Chem.* **2017**, *230*, 448–453. [CrossRef]
22. Wang, H.; Qu, B.; Liu, H.; Ding, J.; Ren, N. Analysis of Organochlorine Pesticides in Surface Water of the Songhua River Using Magnetoliposomes as Adsorbents Coupled with GC-MS/MS Detection. *Sci. Total Environ.* **2018**, *618*, 70–79. [CrossRef]
23. Aslantas, S.; Golge, O.; González-Curbelo, M.Á.; Kabak, B. Determination of 355 Pesticides in Lemon and Lemon Juice by LC-MS/MS and GC-MS/MS. *Foods* **2023**, *12*, 1812. [CrossRef] [PubMed]
24. Liu, W.; Quan, J.; Hu, Z. Detection of Organophosphorus Pesticides in Wheat by Ionic Liquid-Based Dispersive Liquid-Liquid Microextraction Combined with HPLC. *J. Anal. Methods Chem.* **2018**, *2018*, 8916393. [CrossRef] [PubMed]
25. Albanis, T.A.; Hela, D.G. Multi-Residue Pesticide Analysis in Environmental Water Samples Using Solid-Phase Extraction Discs and Gas Chromatography with Flame Thermionic and Mass-Selective Detection. *J. Chromatogr. A* **1995**, *707*, 283–292. [CrossRef]
26. Louca Christodoulou, D.; Kourouzidou, O.; Hadjigeorgiou, M.; Hadjiloizou, P.; Constantinou, M.; Constantinou, P.; Kika, K.; Klavarioti, M. Multi-Residue Analysis of Pesticide Residues in Fruits and Vegetables Using Gas and Liquid Chromatography with Mass Spectrometric Detection. *Accredit. Qual. Assur.* **2018**, *23*, 145–175. [CrossRef]
27. Ma, T.; Zhou, J.; Wei, D.; Peng, H.; Liu, X.; Guo, W.; Zhang, C.; Liu, X.; Li, S.; Deng, Y. Ultrasensitive Electrochemical Aptasensing of Malathion Based on Hydroxylated Black Phosphorus/Poly-L-Lysine Composite. *Biosensors* **2023**, *13*, 735. [CrossRef] [PubMed]
28. Alonso-Lomillo, M.A.; Dominguez-Renedo, O.; Matos, P.; Arcos-Martinez, M.J. Disposable Biosensors for Determination of Biogenic Amines. *Anal. Chim. Acta* **2010**, *665*, 26–31. [CrossRef] [PubMed]
29. Lukowiak, A.; Strek, W. Sensing Abilities of Materials Prepared by Sol–Gel Technology. *J. Solgel Sci. Technol.* **2009**, *50*, 201–215. [CrossRef]
30. Umapathi, R.; Park, B.; Sonwal, S.; Rani, G.M.; Cho, Y.; Huh, Y.S. Advances in Optical-Sensing Strategies for the on-Site Detection of Pesticides in Agricultural Foods. *Trends Food Sci. Technol.* **2022**, *119*, 69–89. [CrossRef]
31. Li, W.-K.; Feng, J.-T.; Ma, Z.-Q. Nitrogen, Sulfur, Boron and Flavonoid Moiety Co-Incorporated Carbon Dots for Sensitive Fluorescence Detection of Pesticides. *Carbon* **2020**, *161*, 685–693. [CrossRef]
32. Zhang, B.; Li, B.; Wang, Z. Creation of Carbazole-Based Fluorescent Porous Polymers for Recognition and Detection of Various Pesticides in Water. *ACS Sens.* **2020**, *5*, 162–170. [CrossRef]
33. Cheng, N.; Song, Y.; Fu, Q.; Du, D.; Luo, Y.; Wang, Y.; Xu, W.; Lin, Y. Aptasensor Based on Fluorophore-Quencher Nano-Pair and Smartphone Spectrum Reader for on-Site Quantification of Multi-Pesticides. *Biosens. Bioelectron.* **2018**, *117*, 75–83. [CrossRef] [PubMed]
34. Hu, T.; Xu, J.; Ye, Y.; Han, Y.; Li, X.; Wang, Z.; Sun, D.; Zhou, Y.; Ni, Z. Visual Detection of Mixed Organophosphorous Pesticide Using QD-AChE Aerogel Based Microfluidic Arrays Sensor. *Biosens. Bioelectron.* **2019**, *136*, 112–117. [CrossRef] [PubMed]

35. Shin, Y.-H.; Teresa Gutierrez-Wing, M.; Choi, J.-W. Review—Recent Progress in Portable Fluorescence Sensors. *J. Electrochem. Soc.* **2021**, *168*, 017502. [CrossRef]
36. Wu, D.; Sedgwick, A.C.; Gunnlaugsson, T.; Akkaya, E.U.; Yoon, J.; James, T.D. Fluorescent Chemosensors: The Past, Present and Future. *Chem. Soc. Rev.* **2017**, *46*, 7105–7123. [CrossRef] [PubMed]
37. Nie, Y.; Teng, Y.; Li, P.; Liu, W.; Shi, Q.; Zhang, Y. Label-Free Aptamer-Based Sensor for Specific Detection of Malathion Residues by Surface-Enhanced Raman Scattering. *Spectrochim. Acta A Mol. Biomol. Spectrosc.* **2018**, *191*, 271–276. [CrossRef] [PubMed]
38. Liang, N.; Hu, X.; Li, W.; Mwakosya, A.W.; Guo, Z.; Xu, Y.; Huang, X.; Li, Z.; Zhang, X.; Zou, X.; et al. Fluorescence and Colorimetric Dual-Mode Sensor for Visual Detection of Malathion in Cabbage Based on Carbon Quantum Dots and Gold Nanoparticles. *Food Chem.* **2021**, *343*, 128494. [CrossRef] [PubMed]
39. Bala, R.; Swami, A.; Tabujew, I.; Peneva, K.; Wangoo, N.; Sharma, R.K. Ultra-Sensitive Detection of Malathion Using Quantum Dots-Polymer Based Fluorescence Aptasensor. *Biosens Bioelectron* **2018**, *104*, 45–49. [CrossRef]
40. Zhai, W.; Cao, M.; Xiao, Z.; Li, D.; Wang, M. Rapid Detection of Malathion, Phoxim and Thiram on Orange Surfaces Using Ag Nanoparticle Modified PDMS as Surface-Enhanced Raman Spectroscopy Substrate. *Foods* **2022**, *11*, 3597. [CrossRef]
41. Azab, H.A.; Ibrahim, I.A.; Hassan, N.; Abbas, A.M.; Darwish, H.M. Synthesis and Photo-Physical Properties of Novel Tb(III)-[Ethyl-4-Hydroxy-1-(4-Methoxyphenyl)−2-Quinolinone-3-Carboxylate] Complex and Luminescence Sensitivity towards Malathion and Crotoxyphos Pesticides. *J. Lumin.* **2017**, *192*, 376–384. [CrossRef]
42. Azab, H.A.; Kamel, R.M. Binding of Chlorfenvinphos and Malathion with DNA and Their Detection Using New Sensitive Luminescent Tb(III) Complex Probe. *J. Lumin.* **2016**, *170*, 671–678. [CrossRef]
43. Azab, H.A.; Anwar, Z.M.; Rizk, M.A.; Khairy, G.M.; El-Asfoury, M.H. Determination of Organophosphorus Pesticides in Water Samples by Using a New Sensitive Luminescent Probe of Eu (III) Complex. *J. Lumin.* **2015**, *157*, 371–382. [CrossRef]
44. Azab, H.A.; Duerkop, A.; Anwar, Z.M.; Hussein, B.H.M.; Rizk, M.A.; Amin, T. Luminescence Recognition of Different Organophosphorus Pesticides by the Luminescent Eu(III)–Pyridine-2,6-Dicarboxylic Acid Probe. *Anal. Chim. Acta* **2013**, *759*, 81–91. [CrossRef] [PubMed]
45. Hasegawa, Y.; Wada, Y.; Yanagida, S. Strategies for the Design of Luminescent Lanthanide(III) Complexes and Their Photonic Applications. *J. Photochem. Photobiol. C Photochem. Rev.* **2004**, *5*, 183–202. [CrossRef]
46. Parker, D.; Dickins, R.S.; Puschmann, H.; Crossland, C.; Howard, J.A.K. Being Excited by Lanthanide Coordination Complexes: Aqua Species, Chirality, Excited-State Chemistry, and Exchange Dynamics. *Chem. Rev.* **2002**, *102*, 1977–2010. [CrossRef] [PubMed]
47. Montalti, M.; Prodi, L.; Zaccheroni, N.; Charbonnière, L.; Douce, L.; Ziessel, R. A Luminescent Anion Sensor Based on a Europium Hybrid Complex. *J. Am. Chem. Soc.* **2001**, *123*, 12694–12695. [CrossRef] [PubMed]
48. Richardson, F.S. Terbium(III) and Europium(III) Ions as Luminescent Probes and Stains for Biomolecular Systems. *Chem. Rev.* **1982**, *82*, 541–552. [CrossRef]
49. Thibon, A.; Pierre, V.C. Principles of Responsive Lanthanide-Based Luminescent Probes for Cellular Imaging. *Anal. Bioanal. Chem.* **2009**, *394*, 107–120. [CrossRef]
50. de Bettencourt-Dias, A. *Luminescence of Lanthanide Ions in Coordination Compounds and Nanomaterials*; de Bettencourt-Dias, A., Ed.; John Wiley & Sons Ltd.: Hoboken, NJ, USA, 2014; ISBN 9781118682760.
51. Kubeil, M.; Martínez, I.; Bachmann, M.; Kopka, K.; Tuck, K.; Stephan, H. Dual-Labelling Strategies for Nuclear and Fluorescence Molecular Imaging: Current Status and Future Perspectives. *Pharmaceuticals* **2022**, *15*, 432. [CrossRef]
52. Zhao, G.-J.; Han, K.-L. Role of Intramolecular and Intermolecular Hydrogen Bonding in Both Singlet and Triplet Excited States of Aminofluorenones on Internal Conversion, Intersystem Crossing, and Twisted Intramolecular Charge Transfer. *J. Phys. Chem. A* **2009**, *113*, 14329–14335. [CrossRef]
53. Ceba, M.R.; Blanco, C.C.; Sánchez, F.G. Solvent Effects on Electronic Absorption and Fluorescence Spectra of Salicylaldehyde 2-Pyridylhydrazone and Indolaldehyde 2-Salicylhydrazone: Ground and Excited State Dissociation Constants. *J. Photochem.* **1985**, *30*, 353–362. [CrossRef]
54. Ressalan, S.; Iyer, C.S.P. Absorption and Fluorescence Spectroscopy of 3-Hydroxy-3-Phenyl-1-o-Carboxyphenyltriazene and Its Copper (II), Nickel (II) and Zinc (II) Complexes: A Novel Fluorescence Sensor. *J. Lumin.* **2005**, *111*, 121–129. [CrossRef]
55. Ibrahim, I.A.; Abbas, A.M.; Darwish, H.M. Fluorescence Sensing of Dichlorvos Pesticide by the Luminescent Tb(III)-3-Ally-Salicylohydrazide Probe. *Luminescence* **2017**, *32*, 1541–1546. [CrossRef]
56. Azab, H.A.; Khairy, G.M.; El-Ghany, N.A.; Ahmed, M.A. Time-Resolved Fluorescence Sensing of N-Acetyl Amino Acids, Nucleobases, Nucleotides and DNA by the Luminescent Tb (III)-8-Alkyl-2-Oxo-2H-Chromene-3-Carbaldehyde Probe. *J. Lumin.* **2016**, *176*, 181–192. [CrossRef]
57. Li, Q.; Li, T. Jinguang Wu Luminescence of Europium(III) and Terbium(III) Complexes Incorporated in Poly(Vinyl Pyrrolidone) Matrix. *J. Phys. Chem. B* **2001**, *105*, 12293–12296. [CrossRef]
58. Lehn, J.-M. Perspectives in Supramolecular Chemistry—From Molecular Recognition towards Molecular Information Processing and Self-Organization. *Angew. Chem. Int. Ed.* **1990**, *29*, 1304–1319. [CrossRef]
59. Xu, J.; Huang, X.H.; Zhou, N.L.; Zhang, J.S.; Bao, J.C.; Lu, T.H.; Li, C. Synthesis, XPS and Fluorescence Properties of Eu3+ Complex with Polydimethylsiloxane. *Mater. Lett.* **2004**, *58*, 1938–1942. [CrossRef]
60. Kazakov, V.P.; Voloshin, A.I.; Ostakhov, S.S.; Shavaleev, N.M. The Anomalous Influence of Water on the Intensity and Lifetime of Fluorescence in Tris(Benzoyltrifluoroacetonate)Europium(III). *Mendeleev Commun.* **1998**, *8*, 47–49. [CrossRef]

61. Kleiman, M.; Ryu, K.A.; Esser-Kahn, A.P. Determination of Factors Influencing the Wet Etching of Polydimethylsiloxane Using Tetra-*n*-Butylammonium Fluoride. *Macromol. Chem. Phys.* **2016**, *217*, 284–291. [CrossRef]
62. Wang, S.; Cao, T.; Yan, H.; Li, Y.; Lu, J.; Ma, R.; Li, D.; Dou, J.; Bai, J. Functionalization of Microporous Lanthanide-Based Metal–Organic Frameworks by Dicarboxylate Ligands with Methyl-Substituted Thieno[2,3-*b*]Thiophene Groups: Sensing Activities and Magnetic Properties. *Inorg. Chem.* **2016**, *55*, 5139–5151. [CrossRef]
63. Genovese, D.; Cingolani, M.; Rampazzo, E.; Prodi, L.; Zaccheroni, N. Static Quenching upon Adduct Formation: A Treatment without Shortcuts and Approximations. *Chem. Soc. Rev.* **2021**, *50*, 8414–8427. [CrossRef]
64. Azab, H.A.; Khairy, G.M.; El-Ghany, N.A.; Ahmed, M.A. A New Luminescent Bio-Probe of Europium(III)-Complex for Sensing Some Biomolecules and CT-DNA. *J. Photochem. Photobiol. A Chem.* **2019**, *374*, 1–9. [CrossRef]
65. Meng, Q.; Liu, H.; Sen, C.; Cao, C.; Ren, J. A Novel Molecular Probe Sensing Polynuclear Hydrolyzed Aluminum by Chelation-Enhanced Fluorescence. *Talanta* **2012**, *99*, 464–470. [CrossRef] [PubMed]
66. Lineweaver, H.; Burk, D. The Determination of Enzyme Dissociation Constants. *J. Am. Chem. Soc.* **1934**, *56*, 658–666. [CrossRef]
67. Lima, E.C.; Gomes, A.A.; Tran, H.N. Comparison of the Nonlinear and Linear Forms of the van't Hoff Equation for Calculation of Adsorption Thermodynamic Parameters (ΔS° and ΔH°). *J. Mol. Liq.* **2020**, *311*, 113315. [CrossRef]
68. Ross, P.D.; Subramanian, S. Thermodynamics of Protein Association Reactions: Forces Contributing to Stability. *Biochemistry* **1981**, *20*, 3096–3102. [CrossRef] [PubMed]
69. Alhamami, M.A.M.; Algethami, J.S.; Rizk, M.A.; Abbas, A.M.; Khairy, G.M. A New Chemosensor Based on a Luminescent Complex for the Investigation of Some Organophosphorus Pesticides in Environmental Samples. *Chemosensors* **2022**, *10*, 391. [CrossRef]
70. Rodríguez, L.C.; Campa[nbreve]Ta, A.M.G.; Linares, C.J.; Ceba, M.R. Estimation of Performance Characteristics of an Analytical Method Using the Data Set Of The Calibration Experiment. *Anal. Lett.* **1993**, *26*, 1243–1258. [CrossRef]